RSC Advances

PAPER

View Article Online
View Journal | View Issue

Cite this: *RSC Adv.*, 2017, **7**, 32581

Template-free synthesis of high degree crystallinity zeolite Y with micro–meso–macroporous structure

O. S. Travkina,[ab] M. R. Agliullin,*[ab] N. A. Filippova,[a] A. N. Khazipova,[a] I. G. Danilova,[c] N. G. Grigor'eva,[a] Nama Narender,[d] M. L. Pavlov[a] and B. I. Kutepov[ab]

Received 27th April 2017
Accepted 3rd June 2017

DOI: 10.1039/c7ra04742h

rsc.li/rsc-advances

In this paper a new approach to the creation of a micro–meso–macroporous structure of Y zeolite was proposed. It was based on the selective crystallization into the integral cluster crystals of the preliminarily molded granules containing crystals of the zeolite in question and a porous binder matrix. The synthesized material was characterized by the high crystallinity degree of 95% and the volume of micro-, meso-, and macro-pores of 0.30, 0.15 and 0.15 $cm^3\ g^{-1}$, respectively. It was shown that the Y zeolite with the hierarchical structure in H-form had the total acidity of about 830 $\mu mol\ g^{-1}$ and revealed the high activity and selectivity in the synthesis of pyridines.

1. Introduction

Zeolite-containing materials have become ingrained in the common use of modern heterogeneous catalysis.[1] The synthetic Y zeolite used in catalysis was the product made in the largest scale.[2] That wide-spread occurrence of it in the chemical industry is associated with the presence of strong Brønsted acid sites and the evolved porous structure as well as with its relatively simple and readily accessible synthesis. The main area of its application is modern cracking catalysts. Y zeolite in H-form is also part of the modern catalysts for the hydrocracking, hydroisomerization of n-paraffins, isomerization of xylenes, disproportionation and delalkylation of toluene, and many other processes in the petroleum chemistry and process technology.[3,4]

Due to steric restrictions, the conventional micro-porous molecular sieves failed to achieve an optimum effect in catalytic transformations where the molecular size of either starting materials or products exceeded 10 Å. The creation of materials possessing the micro–meso–macroporous structure that would provide the efficient diffusion of reagents to the active sites and the reverse diffusion of the reaction products formed[5–8] could become a solution to the above problem.

To date the two alternatives of creating the transport meso- and macropores in zeolites were proposed. The first one was based on the application of templates during the process of crystallization, the former being surface-active substances,[9–11] polymers,[12,13] starch,[14] carbon nanotubes,[17] coal aerogel,[18–20] and nanosized $CaCO_3$.[21] The application of templates enabled to form the zeolite mesopores of 0.15 through 0.70 $cm^3\ g^{-1}$ volume and of 100 through 500 $m^2\ g^{-1}$ surface area as well as to control the pore size within the range of 5–40 nm. The drawbacks of the technique were the low accessibility, high cost, and poor crystallinity degree of the materials obtained.

The second option of creating the transport mesopores in zeolites is based on a partial destruction if the zeolite crystalline lattice by means of either steam, acid, or alkaline treatment resulting in the formation of mesopores. For example, the dealumination by the steam heating or acid treatment was proposed in ref. 22–27 and the desilication with alkali in ref. 28–34. Depending on the zeolite structure and composition the above techniques enabled to create the volume of mesopores within the range of 0.12–0.50 $cm^3\ g^{-1}$, the surface area of mesopores within the range of 100–400 $m^2\ g^{-1}$ and adjust the pore size within the range of 5–40 nm. Despite the accessibility and the ease of use the techniques in question were characterized by such drawbacks as the decreased acidity and crystallinity of the starting material as the result of the dealumination and desilication, as well as a large quantity of acidic and alkaline effluents.

As such, at the moment there were no accessible methods that would enable the creation of micro–meso–macroporous zeolite-based materials possessing the high crystallinity degree and acidity without templates and various post-synthesis treatments. Therefore development of the template-free technique for the synthesis of those materials is the important and

[a]*Federal State Budget Institution of Science, Institute of Petrochemistry and Catalysis of Russian Academy of Sciences, 141 Pr. Oktyabrya, Ufa 450075, Russian Federation. E-mail: MaratRadikovich@mail.ru; Fax: +7 347 231 27 50*

[b]*Ufa State Petroleum Technological University, 1 Kosmonavtov Street, Ufa, 450062, Russia*

[c]*Boreskov Institute of Catalysis SB RAS, Pr. Lavrentieva 5, 630090 Novosibirsk, Russia*

[d]*CSIR – Indian Institute of Chemical Technology, Uppal Road, Tarnaka, Hyderabad – 500 007, Telangana State, India*

relevant issue for the heterogeneous acid–base catalysis. The proposed in this work approach to the creation of granulated materials based on the high crystallinity degree Y zeolite was free of the disadvantages indicated above.

It was illustrated that materials based on zeolite Y of high degree of crystallinity with a micro–meso–macroporous structure may be used as promising catalysts for the synthesis of pyridines, in particular 3,5-dimethylpyridine. This compound is an important intermediate in the synthesis of antiulcer medicines (omeprazole, lansoprazole, rabeprazole),[35,36] corrosion inhibitors, used as a high-temperature solvent[37,38] and a catalyst for epoxide crosslinking,[38] synthesis of sulfamides,[39] hydroesterification of 1-heptene,[40] synthesis of dimethylsuccinate.[41] 3,5-Lutidine was synthesized with the yield up to 54.7% by the interaction of propionaldehyde, formaldehyde with ammonia in the presence of aluminosilicates promoted by ammonium halides.[42] The authors[43] used zeolite H-ZSM-5, modified with various metals (Pb, Pt, Pd, Sm, La, Ti/K, Fe/Cr) in the same reaction. Typically over H-ZSM-5 (Si/A1 = 150), at 400 °C, the yield of 3,5-lutidine was 63.1 wt% at 66.2% conversion of propionaldehyde. The experiment[44] describes the selective preparation of 3,5-dimethylpyridine by reaction of propanol, formaldehyde, methanol and ammonia in the presence of modified ZSM-5 zeolites. Over LaZSM-5 (Si/AI = 15), at 400 °C the selectivity of 3,5-lutidine is 72.2% at 88.6% conversion of propanol.

In this article we describe the selective synthesis of 3,5-dimethylpyridine from propanol, formaldehyde and ammonia on a sample of meso-HY zeolite (60).

2. Experimental

2.1 Materials and reagents

Sodium silicate ($Na_2SiO_3 \cdot 9H_2O$, 44%, ACROS Organics), sodium aluminate ($NaAlO_2 \cdot 6H_2O$, 55%, Reachim), sodium hydroxide (NaOH, 98%, Reachim), kaolin ($Al_2O_3 \cdot 2SiO_2 \cdot 2H_2O$, 99%, Reachim), and distilled water were used as the basic reagents without any preliminary purification.

2.2 Synthesis of the micro-porous NaY zeolite

NaY zeolite was crystallized from an amorphous alkaline aluminosilicate gel prepared by mixing sodium silicate, sodium aluminate, and sodium hydroxide solutions. The synthesis was performed from the reaction mix of the following composition: $2.5Na_2O \cdot Al_2O_3 \cdot 7SiO_2 \cdot 220H_2O$ at 98–100 °C for 94–96 h. Upon completion of the synthesis the solid phase was separated from the mother liquor, washed off from the excess of alkali to the pH of ~8.0–9.0, and dried at 140–150 °C.

2.3 Synthesis of the hierarchical Y zeolite

The synthesis of the hierarchical Y zeolite was performed by the crystallization of the preliminarily molded granules of $d = 1.1$ mm and $l = 3.6$ mm. The granules for the crystallization were prepared by mixing NaY zeolite with the kaolin binder in the VINCI Technologies MX 0.4 mixer followed by the granulation of the obtained mix using the VINCI Technologies VTE1 extruder. The NaY zeolite content in the starting granule amounted 30 and 60% by mass, and the binder material content was 70% and 40% by mass, respectively. The obtained granules were dried in the atmosphere of air at 30 °C for 24 h followed by the calcination at 650 °C for 4 h. During the calcination the amorphization of kaolin in the granule composition occurred and the granules gained the mechanical strength. The calcined samples with the zeolite content of 30% and 60% by mass were designated as NaY-binder(30) and NaY-binder(60), respectively. The calcined granules of NaY-binder(30) and NaY-binder(60) were subjected to the crystallization at 90–100 °C for 46–52 h in a sodium silicate solution, the reaction mix composition being $2.5Na_2O \cdot Al_2O_3 \cdot 6.5SiO_2 \cdot 160H_2O$. After the crystallization the granules were separated form the liquid phase, washed off from the excess of alkali to the pH of ~8.0–9.0, and dried at 140–150 °C. The Y zeolite samples in H-form were prepared by means of the ion exchange of Na^+ cations to NH_4^+ cations in the aqueous 70 g L^{-1} of ammonium nitrate solution (to provide the excess of the exchanging cation) under stirring at 70–90 °C for 1 h. Upon completion of the ion exchange the sample was dried at 120–150 °C and calcined at 540–550 °C for 4 h in the atmosphere of dry air.

The powdered NaY zeolite sample was designated as micro-Y. The granulated samples of Y zeolite synthesized from the starting NaY-binder(30) and NaY-binder(60) granules containing 30% and 60% of the crystalline phase, respectively, were designated as NaY-mmm(30) and NaY-mmm(60). After the conversion of the Na-form into the H-form the H index was added to the sample notation.

2.4 Physical and chemical studies of the obtained materials

The chemical composition of the prepared aluminosilicates was analyzed on a EDX-720/900HS Shimadzu X-ray fluorescent spectrometer.

Diffraction patterns were recorded using Ultima IV "Rigaku" diffractometer in the monochromatic CuKα emission within the 2θ angle range of 3 to 50 in 0.5 deg min^{-1} increments and the 20 s integration time at each point. The relative crystallinity degree was evaluated by the summation of areas of 5 the most intensive peaks. The X-ray phase studies were performed by matching the diffraction patterns obtained with the pdf 2 (Rigaku) database.

The coordination sphere of aluminum atoms in the calcined samples was evaluated by the ^{27}Al MAS NMR spectra. The spectra were obtained using Avance-400 "Bruker" spectrometer equipped with the multi-nuclear sensor in the simple single pulse experiment under the ~104 Hz magic angle spinning of the samples in zirconium dioxide rotors. The aqueous 1 mol L^{-1} $AlCl_3$ solution was used for the external reference standard.

Samples morphology was studied under native conditions to exclude metal coating surface effects. The observations were carried out using Hitachi SU8000 field-emission scanning electron microscope (FE-SEM). Images were acquired in secondary electron mode at 1 kV accelerating voltage and at working distance 3–4 mm.

The porous structure was characterized by the low temperature (77 K) nitrogen adsorption–desorption using the ASAP-2020 "Micromeritics" sorption meter. Prior to the analysis the samples were vacuum-treated at 350 °C for 6 h. The specific surface area was calculated by the BET method at the relative partial pressure of $P/P_0 = 0.2$. The pore size distribution was calculated by the BJH (Barrett–Joyner–Halenda) desorption curve; the total pore volume was determined by the BJH method at the relative partial pressure of $P/P_0 = 0.95$. The volume of the micropores in the presence of mesopores was determined by means of the *t*-method of de Boer and Lippens.[45]

The total volume of the macropores of 50 nm size and larger was evaluated by the mercury injection porosimetry using the Carlo Erba Porozimetr-2000 instrument.

Acid properties of aluminosilicates were studied by the temperature programmed desorption of ammonia[46] (TPD NH_3) and infrared spectroscopy (IR-spectroscopy) using the low temperature adsorption of the CO probe molecule.

The acidic properties of zeolites were studied by IR spectroscopy with the use of the low temperature adsorption of CO molecule. IR spectra were recorded on a Shimadzu FTIR-8300 spectrometer within the spectral range of 700–6000 cm^{-1} with a resolution of 4 cm^{-1}. The powder samples were pressed into thin self-supporting wafers (0.010–0.013 g cm^{-2}) and activated in the special quartz IR cell at 823 K for 2 h in dynamic vacuum of 10^{-3} mbar. CO was introduced at liquid nitrogen temperature by doses up to an equilibrium pressure of 13 mbar. The strength of Brønsted acid sites (BAS) was estimated by the method of hydrogen bonds based on the change in the stretching vibration frequency of the OH groups that occurred under CO absorption.

The higher the shift of IR band of OH stretching vibration of the hydroxyls groups ($\Delta\nu_{OH\cdots CO}$), the stronger is the acidity of OH group. After deconvolution of the corresponding IR bands into individual Gauss components by home-made program, the concentration of BAS was determined from the integral intensity of the band attributed to corresponding OH-group in the H-complexes with the CO molecules using the molar integral absorption coefficient $A_0 = 54$ cm μmol^{-1} for the complexes with $\nu_{OH}^{OH\cdots CO}$ 3300–3330 cm^{-1}.[47]

The concentration of Lewis acid sites (LAS) was evaluated from the integral intensity of CO band in the range of 2190–2233 cm^{-1} (A_0, cm μmol^{-1}: 1.23 (2233–2223 cm^{-1}), 1.1 (2216–2206 cm^{-1}), 0.9 (2200–2190 cm^{-1})).[48,49] In the presented spectra, the absorbance was normalized to sample wafer density.

2.5 Catalytic properties of the materials obtained

Prior to the catalytic tests the zeolite samples were subjected to the thermal treatment in the atmosphere of air at 540 °C for 3 h. The synthesis of pyridines by the interaction of propanol with formaldehyde and ammonia was performed in a flow reactor with the fixed catalyst bed of $V = 1$ cm^3 under the barometric pressure, at 300–400 °C, the weight hourly space velocity w of 2–7 h^{-1}, and the C_3H_7OH-to-CH_2O-to-NH_3 molar ratio equal to 1.0 : 0.8 : 1.5. The reaction products were analyzed by GLC on a chromatograph fitted with a flame-ionisation detector (25 m long glass capillary column, SE-30 phase, oven temperature of 50–280 °C, programmed heating at a rate of 8 °C min^{-1}, detector temperature of 250 °C, evaporator temperature of 300 °C, helium carrier gas flowing at a rate of 30 mL min^{-1}).

3. Results and discussion

3.1 Chemical composition and crystallinity of the materials obtained according to the X-ray phase analysis and NMR data

It was found that the Si-to-Al atomic ratio in all the synthesized samples of Y zeolite was close to 10 (Table 1).

In Fig. 1 the XRD patterns of the synthesized samples were given. For all the samples the signals observed were characteristic just of Y zeolite.

The obtained results witnessed a high phase purity of the obtained materials. The NaY, NaY-mmm(30), and NaY-mmm(60) samples were characterized by the crystallinity degree close to 100%, 95%, and 95%, respectively (Table 1).

Ion exchange of Na^+ cations for H^+ does not change the Si : Al ratio and the degree of crystallinity for all samples. It is noteworthy that in most works on the synthesis of hierarchical zeolites including those based on zeolite Y, it is rarely possible to produce a material with a high degree of crystallinity, as a rule, it does not exceed 70%.[9–34]

It was known[1] that the presence of the extra-framework aluminum atoms in the zeolite resulted in the occurrence of the additional signal of 3 through 10 ppm in the MAS NMR ^{27}Al spectra. In Fig. 2 the MAS NMR ^{27}Al spectra of the synthesized samples were shown. It was seen that for the NaY sample just one signal of 50 through 60 ppm was observed, characteristic of the aluminum atoms in the tetrahedral oxygen coordination. For the NaY-mmm(30) and NaY-mmm(60) samples apart from the basic signal of 50 through 70 ppm, a weak signal of 0 through 20 ppm was observed; that was a reflection of some part of the extra-framework aluminum atoms present.

An insignificant increase in the fraction of the signal from 0 to 20 ppm is observed in the transition from the Na-form to the H-form of the zeolite, which is apparently associated with a slight dealumination of the crystal lattice and the appearance of aluminum atoms in the octahedral coordination.

3.2 Porous structure of the obtained materials

In Fig. 3 the nitrogen adsorption–desorption isotherms and the pore size distribution for the NaY-mmm(30) and NaY-mmm(60)

Table 1 Chemical compositions and degree crystallinity of zeolite Y

Sample	Chemical compositions, (mol)	Degree of crystallinity, (%)
NaY	$Si_{10.21}Al_{1.00}$	100
NaY-mmm(30)	$Si_{10.12}Al_{1.00}$	95
NaY-mmm(60)	$Si_{10.41}Al_{1.00}$	95
HY	$Si_{10.12}Al_{1.00}$	100
HY-mmm(30)	$Si_{10.48}Al_{1.00}$	94
HY-mmm(60)	$Si_{10.39}Al_{1.00}$	95

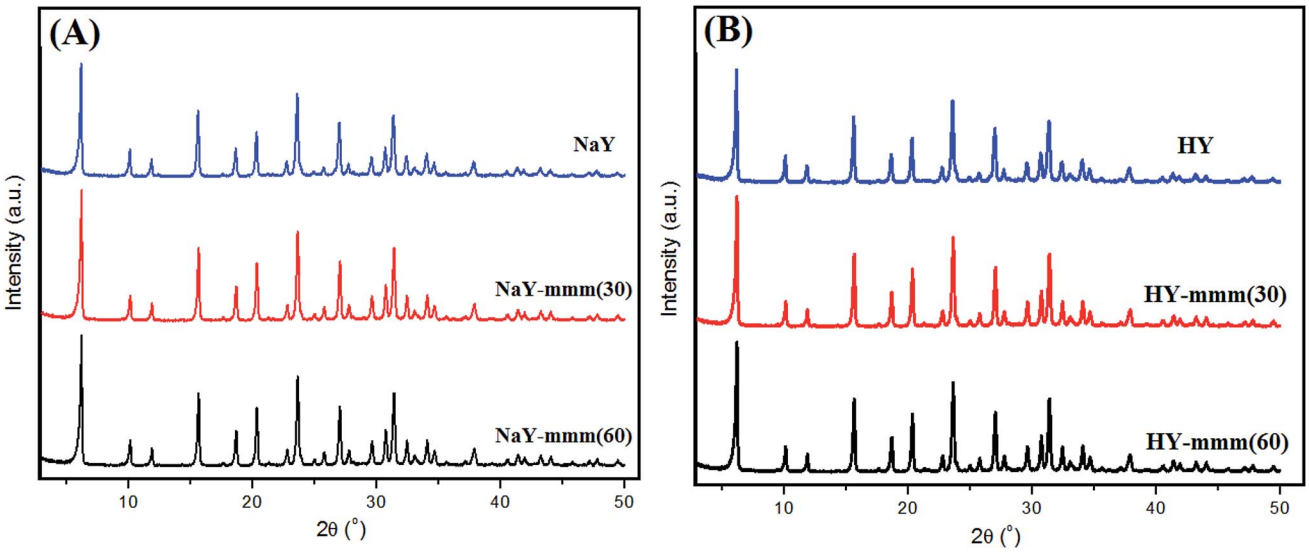

Fig. 1 Powder X-ray diffraction of zeolites Y, (A) Na-form (B) H-form.

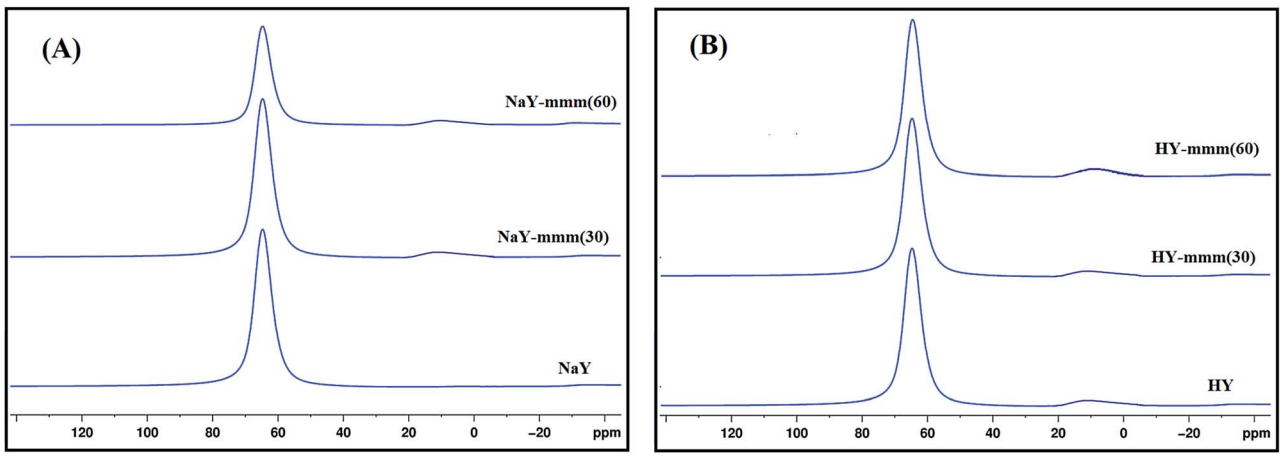

Fig. 2 ^{27}Al MAS NMR spectra of zeolites Y, (A) Na-form (B) H-form.

samples were shown. It is seen that for the NaY-type sample the isotherm of the type I, characteristic of the microporous materials is observed. For the NaY-mmm(30) sample the obtained isotherm was close to the type I. But a hysteresis loop present in the pressure range of 0.8 through 1.0 witnessed the occurrence of the large mesopores. For the NaY-mmm(60) sample the type IV isotherm was observed yet, with the hysteresis loop of N1 type of the IUPAC classification, having an abrupt climb at the pressure of $P/P_0 \sim 1$, characteristic of the meso–macroporous materials. It should be noted that for the NaY-mmm(30) and NaY-mmm(60) samples there was also the characteristic abrupt climb at low temperatures being a reflection of the presence of macropores. The size of the mesopores determined by the BJH method was within the range of 10 through 30 nm for the NaY-mmm(30) sample and within the range of 20 through 30 nm for the NaY-mmm(60) sample (Fig. 3). Similar isotherms of nitrogen adsorption and pore size distribution are also observed for the HY, HY-mmm(30) and HY-mmm(60) samples.

In Table 2 the porous structure characteristics were given according to the data of the nitrogen adsorption–desorption and the mercury injection porosimetry. It is seen that according to the BET method the NaY sample is characterized by the micropore volume of 0.30 $cm^3\ g^{-1}$ and the surface area of 909 $m^2\ g^{-1}$. The results obtained were in good agreement with the reference data for this zeolite reported in ref. 1. The NaY-mmm(30) sample had the specific surface of 791 $m^2\ g^{-1}$ and the volume of micro-, meso-, and macropores of 0.28, 0.05, and 0.14 $cm^3\ g^{-1}$, respectively. The porous structure of the NaY-mmm(60) sample was characterized by the specific surface of 741 $m^2\ g^{-1}$ and the volume of micro-, meso-, and macropores of 0.28, 0.15, and 0.15 $cm^3\ g^{-1}$, respectively.

It must be pointed out that the characteristics of the porous structure basically do not change during the transition from Na-form to H-form for all samples.

Thus, the porous structure of the NaY-mmm(30) sample was formed primarily from micro- and macro-pores. For the NaY-mmm(60) sample the characteristic hierarchical porous

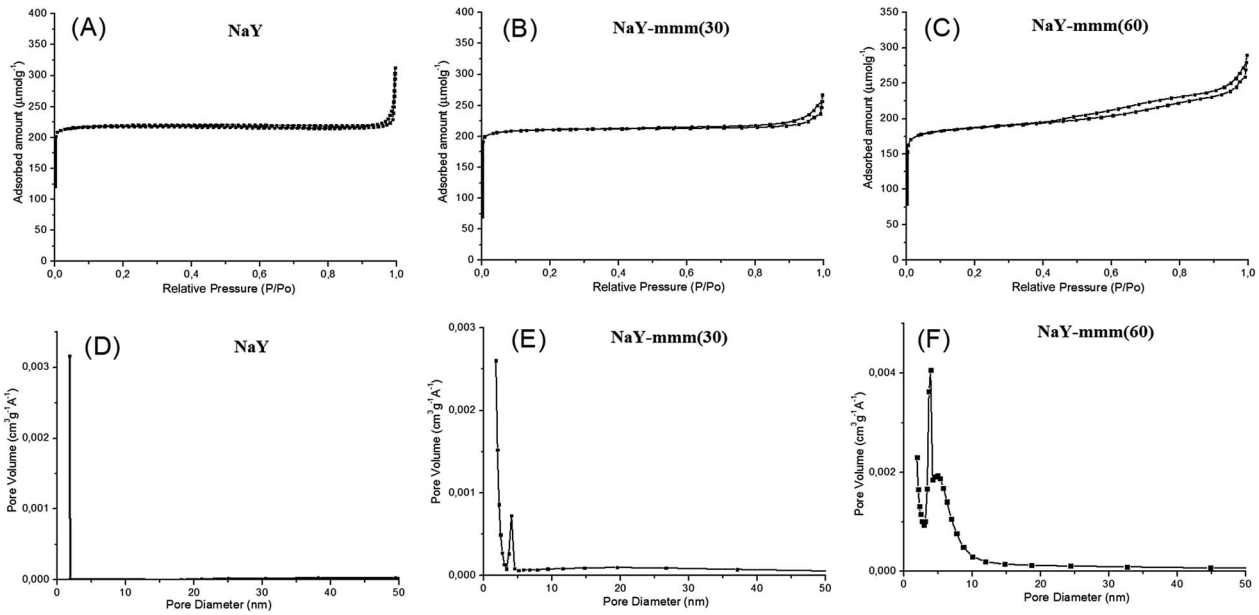

Fig. 3 Nitrogen sorption isotherms and pore size distribution for zeolite Y: (A) micro-NaY; (B) meso-Y(30); (C) meso-Y(60); (D) micro-NaY; (E) meso-Y(30); (F) meso-Y(60).

Table 2 Characteristics of the porous structure

Sample	S_{BET}[a] ($m^2\ g^{-1}$)	V_{micro}[b] ($mL\ g^{-1}$)	V_{meso}[c] ($mL\ g^{-1}$)	V_{macro}[d] ($mL\ g^{-1}$)	V_{Σ}[e] ($mL\ g^{-1}$)
NaY-binder(30)	282	0.09	0.01	0.52	0.62
NaY-binder(60)	550	0.18	0.18	0.50	0.86
NaY	909	0.30	0.03	—	0.33
NaY-mmm(30)	791	0.28	0.05	0.14	0.47
NaY-mmm(60)	741	0.28	0.15	0.15	0.58
HY	899	0.30	0.03	—	0.33
HY-mmm(30)	798	0.28	0.05	0.14	0.47
HY-mmm(60)	735	0.28	0.15	0.15	0.58

[a] Conditions: surface area by method BET. [b] Micropore volume. [c] Mesopore volume. [d] Macropore volume. [e] Total volume.

structure contained not only micro-pores, but meso- and macropores, too. It should be emphasized that in the late work on the synthesis of zeolites with the hierarchical porous structure[50–52] the majority of the obtained materials possessed the micro–mesoporous structure with little to no macro-pores.

3.3 Morphology of the materials obtained

In Fig. 4 the NaY and NaY-mmm(60) sample images obtained by means of the scanning electron microscopy at different magnification were given. It is seen that the powdered micro-NaY zeolite crystals have the regular cubic shape and the average size of 2 μm. Except for the starting Y zeolite crystals, in the NaY-mmm(60) sample the nanocrystals within the range of 50–200 nm size were observed.

3.4 Formation mechanism of meso- and macropores in meso-NaY samples

The porous structure of granules subjected to the crystallization in the process of the NaY-mmm(60) sample preparation consisted of micro-pores in the separately taken zeolite crystals and macro-pores located between the separate crystals and the amorphous binder material particles (Table 2). In the course of the amorphous component crystallization these pores disappeared. Meanwhile an additional quantity of micro-pores and the larger sized pores was formed, resulting from the cluster crystal growth. It followed from the results given above that the micro–meso–macroporous structure of the high crystallinity degree NaY zeolite was formed only when the crystallized granules contained a smaller fraction of the amorphous binder than the fraction of the high-dispersed NaY zeolite.

In Fig. 5 the assumed mesopores formation mechanism in the NaY-mmm(60) sample is shown. It was known that the size of crystals formed during the zeolite crystallization process depended on the seed oversaturation degree. The higher the latter, the smaller is the crystal size. Apparently the very high seed oversaturation degrees leading to the formation of the zeolite nanocrystals, mesopores being the cavities between them, occurred during the crystallization of the sample containing 60% by mass of NaY zeolite.

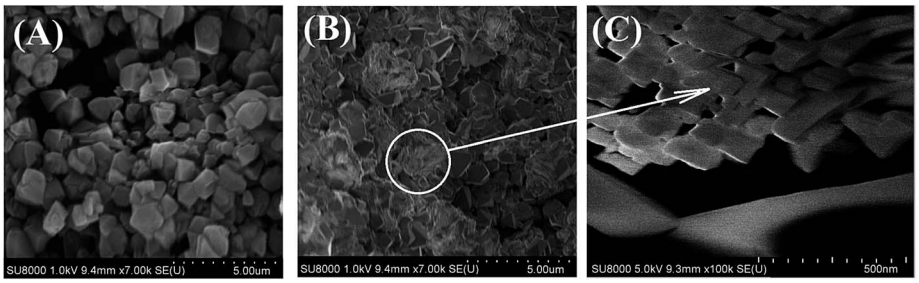

Fig. 4 SEM images of zeolite Y: (A) micro-NaY; (B) meso-Y(60); (C) meso-Y(60).

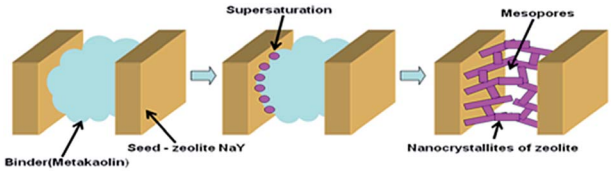

Fig. 5 The mechanism of formation of a hierarchical porous structure in meso-Y(60).

Therefore the primary reason of the mesopore formation in the NaY-mmm(60) sample was the presence of the nanocrystals in the zeolite granule. And the macropores were represented by the cavities formed in the course of the larger crystals clustering.

3.5 Acidity of the materials

According to the TPD NH_3 data (Table 3) the gross acidity values for the HY, HY-mmm(30), and HY-mmm(60) samples amounted 940, 760, and 830 μmol g^{-1}, respectively. A 12–19% decrease in the acidity values of the HY-mmm(60) samples as compared to the HY sample was explained by the fact that they consisted of the integral cluster crystals, which prevented the access of ammonia molecules to a part of the acid sites. It was more characteristic of the HY-mmm(30) sample, though.

The nature of OH-groups over HY and HY-mmm(60) zeolites was studied by FTIR spectroscopy. The IR spectrum of OH groups of HY sample revealed six clearly distinguished bands (Fig. 6).

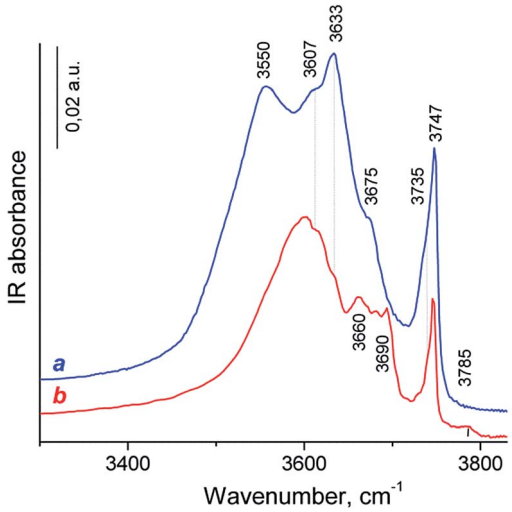

Fig. 6 IR spectra of zeolite samples in the OH region: (a) HY; (b) HY-mmm(60).

The most intense signals at 3747, 3633 and 3550 cm^{-1} were typical for IR spectra of HY zeolites[53–55] and assigned to terminal Si–OH groups and two main kinds of "structural" hydroxyl groups – bridging Si–O(H)–Al groups in the supercages (HF, high frequency) and bridging OH in sodalite cages (LF, low frequency), respectively.

The less intense band at 3607 cm^{-1} was mostly attributed to HF groups polarized by Lewis acidic extraframework Al species (HF′).[54–56] The low intense band at 3675 cm^{-1} can possibly be assigned to the acid Al–O(H)–Al groups which are partially

Table 3 Type and concentration of LAS and BAS according to FTIR spectroscopy of adsorbed CO and TPD NH_3

Type of acid sites	Lewis acid sites		Brönsted acid sites	TPD NH_3
The strength of sites	Strong ν_{CO} = 2231–2223 cm^{-1}	Medium and weak ν_{CO} = 2212–2190 cm^{-1}	Strong ν_{OH} = 3610–3630 cm^{-1} $\Delta\nu_{OH\cdots CO}$ = 300–320 cm^{-1}	Total acid site 150–550 °C

Sample	Concentration (μmol g^{-1})			
HY	33	25	230	940
HY-mmm(60)	21	75	70	830

connected to the framework. The shoulder at 3735 cm^{-1} corresponded to internal or defect silanol OH groups typical for zeolites, which are located in the close vicinity to the lattice imperfection or Lewis acid site (*e.g.*, tricoordinated Al atom, Si–OH···Al^{3+} groups).[57]

The HY-mmm(60) zeolite sample synthesis led to the significant decrease in the signals of bridging OH-groups and to the small decrease in the peak intensity of Si–OH species in the IR spectrum (Fig. 6b). The LF band was shifted to the short-wavelength region to 3600 cm^{-1}. The new bands at 3660, 3680, 3690 and 3785 cm^{-1} were related to the OH-groups bound to the extra-framework aluminum atoms (bridge Al–O(H)–Al and terminal Al–OH groups). This spectrum looked like for those of dealuminated H-Y zeolites.[56,58]

Progressive CO adsorption was carried out on both zeolites. During low temperature CO adsorption on H-Y sample, the HF bands fully disappeared, and a new band at 3330 cm^{-1} appeared, the HF′ band was only partially perturbed, but LF band was not perturbed (the spectrum was not shown). This corresponded to a shift $\Delta\nu_{O-H\cdots CO} = 300\ cm^{-1}$ for HF band, that attributed to strong Brønsted acid sites. This value was lower than for typical dealuminated H-Y zeolites ($\Delta\nu_{O-H\cdots CO}$ = 320–400 cm^{-1}) and slightly higher than for typical H-Y zeolites ($\Delta\nu_{O-H\cdots CO}$ = 270–290 cm^{-1}).[55,59] The appearance of positive bands at 3330 cm^{-1} was accompanied by the broad intense band near at 3400–3450 cm^{-1} and small band at 3595 cm^{-1}. However, the corresponded negative peak for the latter band was not identified. The appearance of the 3400–3450 broad band was caused by the perturbation of the acid OH groups attached to tricoordinated Al atom (bridge Al–O(H)–Al groups with band at 3675 cm^{-1}) and defect acid silanol OH groups (Si–OH···Al^{3+} groups with band at 3735 cm^{-1}). It demonstrates that these groups are less acidic than bridging Si–O(H)–Al groups in faujasite supercages according to the value of the low frequency shift of OH vibrations with adsorbed CO ($\Delta\nu_{O-H\cdots CO}$ = 275–285 cm^{-1}). Besides, the highest pressure of CO close to equilibrium resulted in the shift in the intensity of the silanol bands from 3747 cm^{-1} to *ca.* 3660 cm^{-1}: a shift of ~90 cm^{-1} is typical for weak acidic terminal Si–OH groups.[58,59] The most intense signal in the carbonyl region of IR difference spectra was observed at 2175 cm^{-1}, this band shifted to 2170 cm^{-1} at additional CO dosage. These bands were attributed to the CO complex with strong and moderate acidic OH-groups.[58,59] Additional bands at 2233–2223 cm^{-1} related to CO complexes with Al^{3+} ions in pentahedron environment being specific structure defects of zeolites (strong LAS), low intense bands at 2216–2190 cm^{-1} corresponded to CO complex with extra-framework Al^{3+} species (weak LAS) and band at 2157 cm^{-1} was assigned to CO complex with Si–OH groups.[58]

Progressive low temperature CO adsorption on HY-mmm(60) sample revealed a more complex spectra than that of H-Y sample. During low temperature CO adsorption on HY-mmm(60) sample, the HF and HF′ bands (bridging Si–O(H)–Al groups in faujasite supercages) fully disappeared, and a new band at 3300 cm^{-1} appeared, but LF band at 3600 cm^{-1} was not perturbed (Fig. 7A). It demonstrates that these HF groups are more acidic than those groups in HY-sample according to the value of the low frequency shift of OH vibrations ($\Delta\nu_{O-H\cdots CO}$ = 320 cm^{-1}). The concentration of strong BAS for the zeolite samples was given in Table 3. It could be seen that HY-mmm(60) zeolite contained more than three times less strong BAS in faujasite supercages than HY zeolite. The appearance of positive bands at 3300 cm^{-1} for HY-mmm(60) zeolite was accompanied by the broad band near at 3430–3480 and very intense band at 3500–3520 cm^{-1}. The former signals were caused by the perturbation of the acid OH groups attached to tricoordinated Al atom (bridge Al–O(H)–Al groups with band at 3660 and 3680 cm^{-1}) and defect acid silanol OH groups (Si–OH···Al^{3+} groups with band at 3735 cm^{-1}).

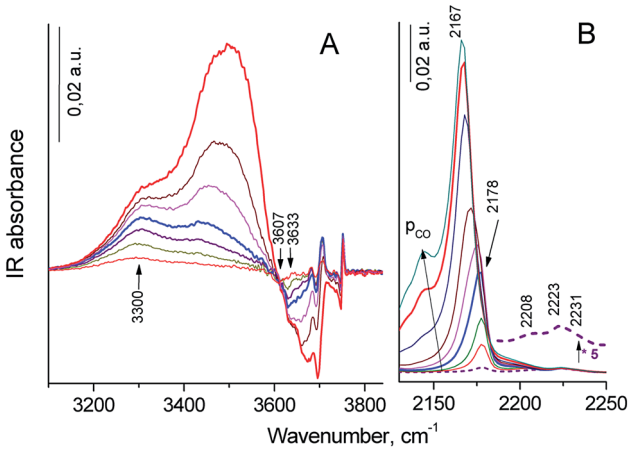

Fig. 7 IR difference spectra in the OH (A) and carbonyl (B) regions between the initial HY-mmm(60) zeolite and those with increased dosage of adsorbed CO from 0.1 (bottom curve) to 4 mbar (top curve) at liquid nitrogen temperature.

The latter peaks were caused by the perturbation of the OH groups with band at 3690–3695 cm^{-1}; the low frequency shift of this OH groups ($\Delta\nu_{O-H\cdots CO}$ = 170–190 cm^{-1}) corresponded to moderate BAS. In the carbonyl region of IR difference spectra it could be observed the intense signal at 2178 cm^{-1} that shifted to 2167 cm^{-1} at additional CO dosage. These bands corresponded to the CO complex with strong and moderate acidic OH-groups (Fig. 7B).[58] According to IR spectra of adsorbed CO in carbonyl region, surface groups in HY-mmm(60) sample contain three types of LAS with following absorbance bands: (1) bands at 2231–2223 cm^{-1} related to CO complexes with Al^{3+} ions in pentahedron environment being specific structure defects of zeolites (strong LAS), (2) low intense bands 2210–2208 cm^{-1} corresponding to LAS of medium strength, (3) bands at 2200–2192 cm^{-1} relating to CO complex with Al^{3+} ions of alumina clusters (weak LAS).[48] The concentration of all types of LAS for the zeolite samples was given in Table 3. It could be seen that HY-mmm(60) zeolite contained three times more moderate and weak LAS deal with extraframework Al species.

3.6 Catalytic properties in the synthesis of pyridines

Catalytic properties of the zeolite HY and meso-HY-mmm(60) samples with the exchange degree of 0.95 were studied in the multicomponent reaction of propanol with formaldehyde and

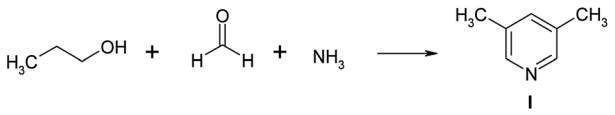

Fig. 8 The reaction scheme for propanol, formaldehyde, and ammonia.

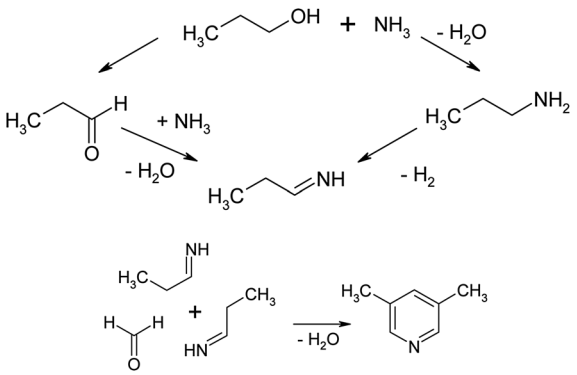

Fig. 9 The possible mechanism of the reaction of propanol with formaldehyde and ammonia.

ammonia at 300–400 °C, at barometric pressure, weight hourly space velocity (w) of 2–7 h^{-1}, and the $C_2H_5OH : CH_2O : NH_3$ molar ratio equal to 1.0 : 0.8 : 1.5 (see Fig. 8).

A possible mechanism for the synthesis of 3,5-dimethylpyridine is described in ref. 44 and is depicted in Fig. 9.

As the authors indicate, the reaction of *n*-propanol with formaldehyde and ammonia proceeds through the intermediate formation of propionaldehyde. Propionaldehyde may form imine by reacting with ammonia.

Two such imines may react with formaldehyde (or methanol) and by cyclization and dehydrogenation lead this compound may to 3,5-lutidine. The active sites for the cyclization and dehydration are Brönsted acidic centres and cations.[60–62]

It was found that 3,5-lutidine (1) was the basic product of the above reaction; the selectivity of its formation reached 90% (Table 4, zeolite HY-mmm(60) zeolite, 300 °C, 7 h^{-1}). 'Light' compounds were present in a small quantity; among them both the linear condensation products of alcohol, formaldehyde and ammonia, such as propylimine, propyl-propenamine and 3-methylpyridine were identified. Beside the lutidine (1), the reaction mass contained 5–23% of 3,4-lutidine and 1–9% of trialkylpyridine (mainly is 2-ethyl-3,5-dimethylpyridine). Under the conditions studied the conversion of propanol on zeolite HY-mmm(60) amounted 35–50%, whereas on HY zeolite it was considerably lower and amounted 16%. The formation selectivity of 63% for 3,5-dimethylpyridine on HY zeolite was also lower than that on HY-mmm(60) zeolite.

The results obtained were associated with the distinctions in the porous structure and the acidic properties of HY zeolite and HY-mmm(60) catalysts. The low activity of HY zeolite could be explained by the rapid blocking of these catalyst micropores by the resulted condensation products, so that the acid sites located inside the large cavities became inaccessible to the reacting molecules. In HY zeolite the multicomponent reaction occurred probably occurred on a few active surface sites and in the pore mouth. As compared to HY-mmm(60) zeolite, the lower selectivity of the 3,5-dimethylpyridine formation could be associated either with the reaction occurred on the surface active sites under no steric constraints imposed on the formation of various reaction products or with the HY zeolite sample acidity.

The Brønsted acid sites (BAS) present in HY zeolite are related to the high acidic bridge Si–O(H)–Al hydroxyl groups located inside the large cavities of the zeolite. There were also the weak acidic OH-groups of the two types bound to the extra-framework aluminum atoms.[63] In HY-mmm(60) zeolite the strong BAS are present both inside the pores and on the external surface of the crystals. The issues associated with the effect of the nature, concentration, and acid site strength studies of HY and HY-mmm(60) zeolites on the selectivity of the alkylpyridine formation demanded more thorough investigation.

The high activity of HY-mmm(60) zeolite in the synthesis of 3,5-dimethylpyridine was reached due to the presence of meso- and macropores in its structure. Such a combined micro–meso–macroporous structure allowed for the reduction of the diffusion constraints imposed on the transport of the reagent and reaction product molecules as well as for the decrease in the possibility of pore blocking. In addition, the concentration of the reacting substances in the mesopores was higher, which led to the increase in the number of the chemical interaction acts between the reagents and subsequently to the higher conversion factor.

Table 4 Synthesis of pyridines on zeolites H-Y, HY-mmm[a]

				Selectivity, %			
Catalyst	T, °C	w, h^{-1}	Conversion of propanol, %	"Light-products"	3,5-Lutidine	3,4-Lutidine	"Heavy-products"
HY-mmm(60)	300	2	41	4	84	7	5
HY-mmm(60)	300	7	35	4	90	5	1
HY-mmm(60)	350	7	40	6	74	13	7
HY-mmm(60)	400	7	50	8	69	14	9
HY	400	7	16	11	63	23	3

[a] Molar ratio – $C_3H_7OH : CH_2O : NH_3 = 1.0 : 0.8 : 1.5$.

4. Conclusions

(1) In this work the technique for building up the hierarchical micro–meso–macroporous structure of the high crystallinity degree NaY zeolite was proposed. The technique is based on the crystallization of granules consisted of the high dispersed NaY zeolite and the amorphous metakaolin binder in the sodium silicate solution at 96–98 °C, provided that the crystalline phase content must be higher than that of the amorphous phase.

(2) The developed technique enables to synthesize the granulated NaY zeolite possessing the crystallinity degree up to 95%, the specific surface area by BET equal to 741 $m^2\ g^{-1}$, and the micro-, meso-, and macropore volume of 0.28, 0.15, and 0.15 $cm^3\ g^{-1}$, respectively. The acidity of its H-form by NH_3 reaches 830 μmol g^{-1}.

(3) It was shown that the primary reason of the mesopore buildup was the formation of the nanodispersed crystals of Y zeolite during the crystallization of the amorphous component in the granules.

(4) It was found that HY-mmm(60) zeolite revealed the high activity and selectivity in the multicomponent reaction of propanol with formaldehyde and ammonia and ensured the production of 3,5-dimethylpyridine with the selectivity of up to 95% and the alcohol conversion factor of 35–40%. The results obtained were considerably superior to those achieved with the microporous HY zeolite.

Acknowledgements

The work was supported by the Russian Science Foundation under grant RSF-DST No. 16-43-02010. The analysis of the obtained compounds was performed with the use of Collective Usage Centre "Agidel" at Institute of Petrochemistry and Catalysis of the Russian Academy of Sciences. Electron microscopy characterisation was performed in the Department of Structural Studies of the Zelinsky Institute of Organic Chemistry, Moscow.

Notes and references

1 J. Cejka, A. Corma and S. Zones, *Zeolites and catalysis: synthesis, reactions and applications*, Wiley-VCH, Weinheim, 2010.
2 T. F. Degnan Jr, *Stud. Surf. Sci. Catal.*, 2007, **170**, 54–65.
3 C. Martínez and A. Corma, *Coord. Chem. Rev.*, 2011, **255**, 1558–1580.
4 W. Vermeiren and J.-P. Gilson, *Top. Catal.*, 2009, **52**, 1131–1161.
5 M. R. Agliullin, I. G. Danilova, A. V. Faizullin, *et al.*, *Microporous Mesoporous Mater.*, 2016, **230**, 118–127.
6 K. Muller and T. Bein, *Chem. Soc. Rev.*, 2013, **42**, 3689–3707.
7 R. Chal, C. Gerardin, M. Bulut and S. Van Donk, *ChemCatChem*, 2011, **3**, 67–81.
8 Y. Wan and D. Zhao, *Chem. Rev.*, 2007, **107**, 2821–2860.
9 M. Choi, H. S. Cho, R. Srivastava, C. Venkatesan, D. H. Choi and R. Ryoo, *Nat. Mater.*, 2006, **5**, 718–723.
10 M. Choi, R. Srivastava and R. Ryoo, *Chem. Commun.*, 2006, 4380–4382.
11 R. Srivastava, M. Choi and R. Ryoo, *Chem. Commun.*, 2006, 4489–4491.
12 F. S. Xiao, L. F. Wang, C. Y. Yin, K. F. Lin, Y. Di, J. X. Li, R. R. Xu, D. S. Su, R. Schlogl, T. Yokoi and T. Tatsumi, *Angew. Chem., Int. Ed.*, 2006, **45**, 3090–3093.
13 H. Wang and T. J. Pinnavaia, *Angew. Chem., Int. Ed.*, 2006, **45**, 7603–7606.
14 C. S. Mei, P. Y. Wen, Z. C. Liu, H. X. Liu, Y. D. Wang, W. M. Yang, Z. K. Xie, W. M. Hua and Z. Gao, *J. Catal.*, 2008, **258**, 243–249.
15 A. H. Janssen, I. Schmidt, C. J. H. Jacobsen, A. J. Koster and K. P. de Jong, *Microporous Mesoporous Mater.*, 2003, **65**, 59–75.
16 C. J. H. Jacobsen, C. Madsen, J. Houzvicka, I. Schmidt and A. Carlsson, *J. Am. Chem. Soc.*, 2000, **122**, 7116–7117.
17 I. Schmidt, A. Boisen, E. Gustavsson, K. Stahl, S. Pehrson, S. Dahl, A. Carlsson and C. J. H. Jacobsen, *Chem. Mater.*, 2001, **13**, 4416–4418.
18 Y. M. Fang, H. Q. Hu and G. H. Chen, *Microporous Mesoporous Mater.*, 2008, **113**, 481–489.
19 Y. S. Tao, H. Kanoh and K. Kaneko, *J. Phys. Chem. B*, 2003, **107**, 10974–10976.
20 Y. S. Tao, H. Tanaka, T. Ohkubo, H. Kanoh and K. Kaneko, *Adsorpt. Sci. Technol.*, 2003, **21**, 199–203.
21 H. Zhu, Z. Liu, Y. Wang, D. Kong, X. Yuan and Z. Xie, *Chem. Mater.*, 2008, **20**, 1134–1139.
22 S. van Donk, A. H. Janssen, J. H. Bitter and K. P. de Jong, *Catal. Rev.: Sci. Eng.*, 2003, **45**, 297–319.
23 B. L. Meyers, T. H. Fleisch, G. J. Ray, J. T. Miller and J. B. Hall, *J. Catal.*, 1988, **110**, 82–95.
24 S. Cartlidge, H. U. Nissen and R. Wessicken, *Zeolites*, 1989, **9**, 346–349.
25 H. Horikoshi, S. Kasahara, T. Fukushima, K. Itabashi, T. Okada, O. Terasaki and D. Watanabe, *Nippon Kagaku Kaishi*, 1989, 398–404.
26 B. Chauvin, P. Massiani, R. Dutartre, F. Figueras, F. Fajula and T. Descourieres, *Zeolites*, 1990, **10**, 174–182.
27 M. Guisnet, Q. L. Wang and G. Giannetto, *Catal. Lett.*, 1990, **4**, 299–302.
28 J. C. Groen, J. A. Moulijn and J. Pérez-Ramírez, *J. Mater. Chem.*, 2006, **16**, 2121–2131.
29 R. M. Dessau, E. W. Valyocsik and N. H. Goeke, *Zeolites*, 1992, **12**, 776–779.
30 G. Lietz, K. H. Schnabel, C. Peuker, T. Gross, W. Storek and J. Völter, *J. Catal.*, 1994, **148**, 562–568.
31 M. Ogura, S. Y. Shinomiya, J. Tateno, Y. Nara, E. Kikuchi and H. Matsukata, *Chem. Lett.*, 2000, 882–883.
32 M. Ogura, S. Y. Shinomiya, J. Tateno, Y. Nara, M. Nomura, E. Kikuchi and M. Matsukata, *Appl. Catal., A*, 2001, **219**, 33–43.
33 T. Suzuki and T. Okuhara, *Microporous Mesoporous Mater.*, 2001, **43**, 83–89.
34 L. L. Su, L. Liu, J. Q. Zhuang, H. X. Wang, Y. G. Li, W. J. Shen, Y. D. Xu and X. H. Bao, *Catal. Lett.*, 2003, **91**, 155–167.

35 S. Shimizu, N. Watanabe, T. Kataoka, T. Shoji, N. Abe, S. Morishita and H. Ichimura, Pyridine and pyridine derivatives, *Encyclopedia of industrial chemistry*, 2012, vol. 30, pp. 558–589.
36 S. Shimizua, N. Abe, A. Iguchi and H. Sato, *Catal. Surv. Jpn.*, 1998, **2**, 71–76.
37 G. D. Henry, *Tetrahedron*, 2004, **60**, 6043–6061.
38 K. S. K. Reddy, K. C. Scrinivasa and K. V. Raghavan, *Catal. Surv. Asia*, 2012, **16**, 28–35.
39 C. Guo, L. Dong, S. Kephart and X. Hou, *Tetrahedron Lett.*, 2010, **51**(21), 2909–2913.
40 C. Jing, F. Hong-xiang and T. Jin, *Fenzi Cuihua*, 2001, **15**(2), 146–148.
41 I. Takahashi, K. Koumoto, A. Matsuda and T. Masuda, *Stud. Polym. Sci.*, 1994, **12**, 596–600.
42 M. Yoshizo and N. Shikibu, *US Pat.* No. 3,946,020, 1976.
43 S. J. Kulkarni, R. Ramachandra Rao and Y. V. Subba Rao, *Appl. Catal., A*, 1996, **136**, 1–6.
44 R. Ramachandra Rao, N. Srinivas, S. J. Kulkarni, M. Subrahmanyam and K. V. Raghavan, *Appl. Catal., A*, 1997, **161**, 37–42.
45 S. J. Gregg and K. S. Sing, *Adsorption, Surface Area, and Porosity*, Academic Press, London, 1995.
46 V. V. Yushchenko, *J. Phys. Chem.*, 1997, **71**, 628.
47 A. V. Toktarev, L. V. Malysheva and E. A. Paukshtis, *Kinet. Catal.*, 2010, **51**, 318–324.
48 E. A. Paukshtis and E. N. Yurchenko, *Russ. Chem. Rev.*, 1983, **52**, 242–258.
49 R. I. Soltanov, E. A. Paukshtis and E. N. Yurchenko, *Kinet. Catal.*, 1982, **23**, 135–141.
50 F. Tian, Q. Shen, Z. Fu, Y. Wu and C. Jia, *Fuel Process. Technol.*, 2014, **128**, 176–182.
51 C. Xinga, G. Yang, M. Wu, R. Yang, L. Tan, P. Zhu, Q. Wei, J. Li, J. Mao, Y. Yoneyama and N. Tsubaki, *Fuel*, 2015, **148**, 48–57.
52 W. Fu, Y. Feng, Z. Fang, Q. Chen, T. Tang, Q. Yu and T. Tang, *Chem. Commun.*, 2016, **52**, 3115–3118.
53 P. A. Jacobs and J. B. Uytterhoeven, *J. Chem. Soc., Faraday Trans.*, 1972, **69**, 359–371.
54 M. W. Anderson and J. Klinowski, *Zeolites*, 1986, **6**, 455–466.
55 S. Kotrel, J. H. Lundsford and H. Knözinger, *J. Phys. Chem. B*, 2001, **105**, 3917–3921.
56 W. Daniell, N. Y. Topsøe and H. Knözinger, *Langmuir*, 2001, **17**, 6233–6239.
57 A. A. Gabrienko, I. G. Danilova, S. S. Arzumanov, A. V. Toktarev, D. Freude and A. G. Stepanov, *Microporous Mesoporous Mater.*, 2010, **131**, 210–216.
58 O. Cairon, T. Chevreau and J.-C. Lavalley, *J. Chem. Soc., Faraday Trans.*, 1998, **94**, 3039–3047.
59 K. Hadjiivanov, *Adv. Catal.*, 2014, **57**, 99–318.
60 R. A. Van Santen, *Stud. Surf. Sci. Catal.*, 1994, **85**, 273–293.
61 S. J. Kulkarni, H. Hattari and K. Tanabe, *Appl. Catal.*, 1989, **49**, 27.
62 V. B. Kazansky, *Stud. Surf. Sci. Catal.*, 1994, **85**, 251–273.
63 N. G. Grigor'eva, N. A. Filippova, M. R. Agliullin, B. I. Kutepov and N. Narender, *J. Chem. Res.*, 2017, **41**(3), 253–261.